ARTICLE

Thermocleavable Materials for Polymer Solar Cells with High Open Circuit Voltage—A Comparative Study

Thomas Tromholt, Suren A. Gevorgyan, Mikkel Jørgensen, Frederik C. Krebs, and Kristian O. Sylvester-Hvid*

Risø National Laboratory for Sustainable Energy, Technical University of Denmark, Frederiksborgvej 399, DK-4000 Roskilde, Denmark

ABSTRACT The search for polymer solar cells giving a high open circuit voltage was conducted through a comparative study of four types of bulk-heterojunction solar cells employing different photoactive layers. As electron donors the thermo-cleavable polymer poly-(3-(2-methylhexyloxycarbonyl)dithiophene) (P3MHOCT) and unsubstituted polythiophene (PT) were used, the latter of which results from thermo cleaving the former at 310 °C. As reference, P3HT solar cells were built in parallel. As electron acceptors, either PCBM or bis-[60]PCBM were used. In excess of 300 solar cells were produced under as identical conditions as possible, varying only the material combination of the photo active layer. It was observed that on replacing PCBM with bis[60]PCBM, the open circuit voltage on average increased by 100 mV for P3MHOCT and 200 mV for PT solar cells. Open circuit voltages approaching 1 V were observed for the PT:bis[60]PCBM solar cells and a maximum conversion efficiency of 1.3% was obtained for solar cells with P3MHOCT:PCBM as the photoactive material. For the reference solar cells maximum efficiencies of 2.1 and 2.4% were achieved for P3HT:PCBM and P3HT:bis[60]PCBM, respectively. Despite special measures taken in terms of substrate design and device processing, a substantial spread in the photovoltaic properties was generally observed. This spread could not be correlated with the optical properties of the solar cells, the thickness of the photo active layer or the electrode deposition conditions of the aluminum top electrode.

KEYWORDS: thermocleavable polymers • high open circuit voltage • P3MHOCT • PT • bis-PCBM

INTRODUCTION

The efficiency optimization of polymer solar cells (1–5) involves detailed studies of the material properties (i.e., band gap, charge carrier mobility, absorption cross-section), the interplay between the material and film forming process, the film morphology dependence on processing (i.e., solvents, drying speed, printing, or coating method) as well as post film formation processes (i.e., solvent annealing, thermal annealing). The search for better suited photoactive materials is therefore challenging and there is no single litmus test for determining if a newly synthesized material will yield improved performance in a given solar cell geometry. An approach normally taken is to make the best of a given set of materials through optimizing deposition techniques, layer sequences, thicknesses, and device architecture in general. In regard to the latter, the use of tandem structures has proven a viable approach to overcome the limitations of using photoactive materials with a limited spectral overlap with the solar spectrum. However, from a processing point of view, the formation of structures with multiple photoactive layers, as well as optical spacer and blocking layers by solution processing has not yet been solved in a satisfactory manner. The obvious problem lies in protecting the first solution processed layer from being redissolved while processing of subsequent layers. The general lack of so-called orthogonal solvent systems for the deposition of different photoactive materials has led to the development of methods that typically employ an oxide, a metal or a PEDOT:PSS layer as the separation layer. For a review of these methods we refer to refs 6 and 7. However, none of these methods seem viable in terms of large-scale roll-to-roll processing, because insertion of inorganic and insoluble separation layers often requires special processing measures, e.g., vacuum deposition.

Photoactive polymers with solubilizing side chains that can be chemically modified or entirely removed by a thermal treatment, that is thermocleavable polymers, may be one way to overcome the problems outlined above. Thermocleavable polymers therefore are highly relevant in the context of polymer-based tandem solar cells, and recently some progress has been made with such materials (8, 9). One such promising candidate is the electron donating polymer poly-(3-(2-methylhexan-2-yl)-oxy-carbonyldithiophene) (P3MHOCT) as reported by Fréchet et al. (10), and later found to allow for fabrication of polymer solar cells with good stability, even under ambient conditions (11–15). Through ^{13}C isotopic labeling coupled with solid-state NMR studies P3MHOCT was found to be cleaved thermally in two subsequent steps as shown in Scheme 1 (16). First, P3MHOCT (pristine or blended with an electron accepting material) undergoes a de-esterfication at 210 °C to yield poly-3-carboxydithiophene (P3CT), which is then decarboxylated at ~300 °C to yield the unsubstituted (or native) poly thiophene (PT). Films of both P3CT and PT are insoluble in organic solvents and thus

* Corresponding author. E-mail: kosh@risoe.dtu.dk.
Received for review August 5, 2009 and accepted November 9, 2009
DOI: 10.1021/am900518r

Published on Web 11/30/2009

Scheme 1. Chemical Transitions Involved in the Thermal Cleaving of P3MHOCT to P3CT and Further from P3CT to PT

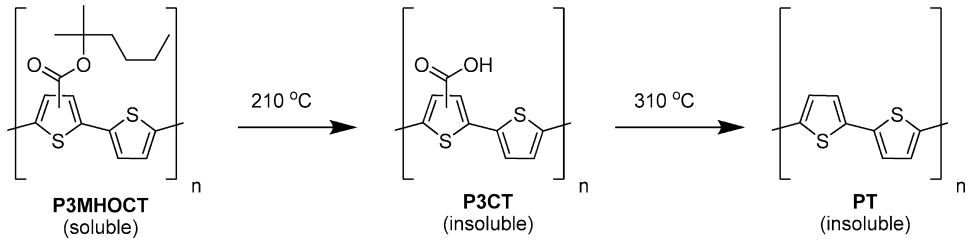

Scheme 2. (A) Layout of the ITO pattern of 50 mm × 50 mm Float Glass Substrates Employed (along the edges of the substrate are all together 16 contact pads, four of which are contacted with the round ITO area available to the solar cells); (B) Evaporation Mask Defining the Four Solar Cells Placed Centrosymmetrically on the Substrate, Each with an Area of 2 cm²

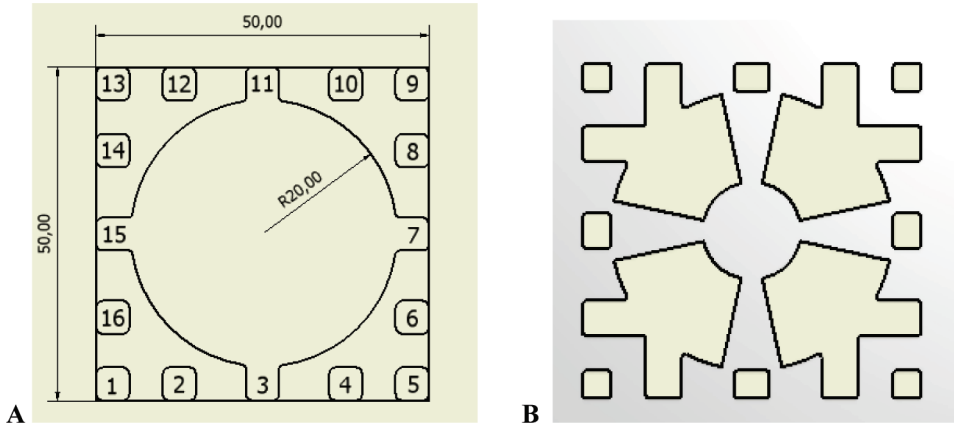

are ideally suited for device structures with multiple photoactive layers as demonstrated, for example, for tandem cells (8). In terms of solar cell efficiency, none of the three materials perform in the range as typical for P3HT, although in the case of PT (in combination with $PC_{70}BM$), bulk-heterojunction solar cells with efficiencies approaching 1.5% have been demonstrated (17).

In this investigation, we extend previous work on the optimization of solar cells based on P3MHOCT and PT and the electron acceptor $PC_{60}BM$ (henceforth referred to as PCBM). Specifically, we investigate the impact on solar cell performance when substituting PCBM with the corresponding bis-adduct (bis-PCBM) as recently used in P3HT solar cells (18). According to cyclic voltammetry (CV), the LUMO of bis-PCBM should be shifted approximately 0.1 eV up in energy relative to the LUMO for PCBM (18). Hence, solar cells with photoactive layers of P3MHOCT:bis-PCBM and PT:bis-PCBM hold the potential for improved performance by virtue of a higher open circuit voltage (V_{oc}). This naturally assumes that neither blend mobilities nor morphology are negatively affected by replacing PCBM with bis-PCBM, as well as the absorption characteristic of the solar cell. To elucidate this, we here present a comparative study of solar cells produced with the P3MHOCT:PCBM, PT:PCBM, P3MHOCT:bis-PCBM and PT:bis-PCBM composites.

Solar cells based on poly(3-hexyl-thiophene) (P3HT) have been found to exhibit a large spread in their photovoltaic properties and efficiency as demonstrated in a study where ~360 identical P3HT:PCBM cells were produced and a statistical analysis performed (19). Even for small area solar cells produced on the same small substrate, a substantial spread in efficiency was observed. When taking this to an industrial process scale, a similar spread was observed for printed solar cells employing the same type of materials (20). In the present comparative study, we consider a large number of solar cells produced under identical conditions, changing only the photoactive composite material. On the basis of the experiences obtained in ref 19, further measures in terms of substrate design are taken in an attempt to decrease the variability of the electrical properties of solar cells.

EXPERIMENTAL SECTION

Device Layout. Photovoltaic devices were prepared on 50 mm by 50 mm patterned ITO (~140 nm) substrates as provided by Luminescence Technology with a thickness of 0.7 mm and a nominal surface resistance of 5−15 Ω/□. The typical surface resistance was about 12 Ω/□. The ITO pattern as shown in Scheme 2A consists of 16 contact pads positioned symmetrically along the substrate edges and a round area with radius of 20 mm centered on the substrate. Four of the contact pads (number 3, 7, 11, and 15) are part of the round ITO area, the latter of which is intended as a general region where any number of solar cells can be positioned, depending on the contacting scheme. The substrate was designed specifically with spin-coating in mind and thus allows solar cells to be positioned and contacted in a centro-symmetric fashion within the round ITO area. Also, the round uninterrupted ITO area allows for a uniform and uninterrupted solution flow during spin-coating procedure, regardless of how the solar cells are laid out on the substrate.

Here we have chosen a device layout with four 2 cm^2 cells laid out centrosymmetrically on the substrate with symmetric and redundant contact structures. The layout is illustrated by the mask used for electrode deposition as shown in Scheme 2B. Hence, under ideal spin-coating conditions (substrate centered on spin chuck and solution deposition centered on substrate) in terms of process geometry, the four cells see identical process conditions. Further, the four solar cells have been positioned such as to maximize the radial distance to the center in order to minimize the radial width of the solar cells while maintaining an area of 2 cm^2. Note that in order to minimize the influence of the radial dependence of the film thickness, in principle, the solar cells should be laid out in as narrow a band as possible.

Device Preparation. The solar cells were prepared according to the following general procedure: Sonication for 10 min in isopropanol and then in demineralized water followed by blow drying. The substrates were flooded with cold (ca. 5 °C) Poly(3,4-ethylenedioxythiophene)-poly(styrenesulfonate) (PEDOT:PSS, 1.3 wt % in H_2O) as supplied from Aldrich and spun at 2800 rpm for 1 min, after which PEDOT:PSS was removed manually from the contact pads. Immediately before PEDOT:PSS spin coating, each substrate was washed with water while spinning at 2800 rpm. Annealing for 1 min at 150 °C was done on a hot plate after which the substrates were transferred to a N_2 glovebox environment (O_2 and H_2O below 0.1 ppm) where the substrates subsequently were annealed for further 5 min at 150 °C on a hot plate. A 0.5 mL blend solution was spin coated using a procedure where the substrate was first spun at 3000 rpm for 30 s, during which the substrate was washed with 0.5 mL *o*-dichlorobenzene, followed by spinning at 800 rpm afterward. The substrates were generally spun until they appeared dry (ca. 4 min) after which the photoactive layer was removed from the contract structure. The resulting films generally appeared very homogeneous always covering the entire substrate, i.e., the P3MHOCT:acceptor solution exhibits very good wetting and flow properties and thus is well-suited for spin coating.

PT devices were obtained by thermally cleaving the P3MHOCT devices on a hot plate at 310 °C in the glovebox right after spin coating. The chemical transition from P3MHOCT to PT is accompanied by two color changes upon heating; first the film changes color from purple to yellow as a characteristic of P3CT formation. Upon further heating, the film again turns purple signifying the formation of PT. The substrates were removed from the hot plate as quickly as possible after the second color change was completed. Note that the color change always evolved as a seeded process. Hence, the devices were always placed on the same place on the same hot plate. Because of the small nonuniformity of the heating of the hot plate the thermal cleaving (i.e., color change) could therefore be made to initiate from the same location on nearly all devices. The thermal cleaving was defined to be complete when the entire film had undergone the last color change.

The above production steps were always performed on a batch of six substrates (24 solar cells) of which three were processed with polymer:PCBM blend and the remaining three with polymer:bis-PCBM blend. Care was taken to minimize the variation of production parameters during the processing of a batch, which typically took about 6 h (characterization included). Immediately following the film-processing (and thermal cleaving for PT devices), all six substrates of the given batch were transferred to an external vacuum chamber where approximately 100 nm Al was deposited at a base pressure of $\sim 2 \times 10^{-6}$ Torr within ~1−2 min, while rotating the substrate holder.

Electrical characterization of the entire batch of solar cells followed immediately thereafter under ambient conditions.

All together 8 batches were processed for the purposes of this study: In batches 1−4,the polymer was PT and these batches are termed PT1 to PT4. In batches 5−8, the uncleaved polymer P3MHOCT was employed and these are termed P3MHOCT1 to P3MHOCT4. Care was also taken not to change any experimental conditions between processing of different batches.

An additional four batches of solar cells (one for each blend combination) were prepared for the purpose of correlating spectral features of the UV−vis spectra of the solar cells with the thickness of the photoactive layer. Each batch consisted of 7 substrates prepared in the same way as described above, but with the blend spin-coating speed and time chosen differently for each substrate (i.e., 300, 400, 500, 600, 800, 1000, or 1200 rpm). The same material combination was used for the entire batch of 7 solar cell substrates. After recording the UV−vis absorption spectra for these additional 28 substrates, each substrate was analyzed by AFM to estimate the thickness of the photoactive layer. This was done by recording step profiles obtained from scanning across a scratch in the film multiple times. For the two batches with PT solar cells, regions where only the blend layer occurred on the substrate (corner regions outside the ITO pattern) were scratched and analyzed. For the P3MHOCT solar cells, regions between the solar-cell pixels were subject to AFM analysis. In this case, double step profiles could always be located, yielding both a PEDOT:PSS and blend layer thickness. In both cases, an average of two AFM step scans were performed per substrate.

For reference, an additional four batches of P3HT:PCBM and P3HT:bis-PCBM solar cells (batches named P3HT1 to P3HT4) with three substrates of each were prepared according to the procedure described above. Following electrode deposition, however, the P3HT based solar cells were thermally annealed at 140 °C for 5 min in the glovebox and subsequently taken out for immediate characterization.

Preparation of Photo Active Solutions. Poly-(3-(2-methylhexan-2-yl)-oxy-carbonyldithiophene) (P3MHOCT) as previously synthesized for a study of large scale production of solar cells was used here (M_n = 11 300, M_w = 36 900, M_p = 29 800, PD = 3.3) (20). PCBM (99%, Lot: 08.01.08) and bis-PCBM (99.9% Lot: 31.01.08 as well as Lot: 15.07.08) both obtained from Solenne BV were used as received. All blend solutions were made from 20 mg of P3MHOCT plus 20 mg of PCBM (or bis-PCBM) per 1 mL of anhydrous *o*-dichlorobenzene, and were stirred overnight at ~40 °C, after which they were filtered cold through 0.45 μm filters. Typically, 20 mL solution was prepared such that all batches could be processed from the same solution. Solutions were always kept stirring at ~40 °C and all handling of the solutions was restricted to the glovebox environment and also deposited at this temperature.

For the P3HT solar cells a blend solution consisting of 10 mg/mL P3HT (Rieke Metals, Lot: BS16−24) and 10 mg/mL PCBM (99% Lot: 29.06.09) or bis-PCBM (99.5% Lot: 11.12.08) in chlorobenzene was used. The solution was stirred at ca. 40 °C overnight, after which it was brought to room temperature and was ready to use. Because of the relativity low concentrations, no filtering was required. The solution was kept under inert atmosphere at constant stirring and deposited at room temperature.

Electrical and Optical Device Characterization. The dark and illuminated IV characteristics of the four solar cells on each substrate were recorded using a substrate holder contacting the contact pads 1−16 (see Scheme 2A) simultaneously. A computer program was employed to automatically switch the relays in a Keithley 2700 multimeter/data acquisition system connecting each solar cell in turn to a Keithley 2400 sourcemeter in a two-wire measurement configuration. The solar cells were contacted in a redundant and symmetric fashion that is, for solar cell 1 contacting the cathode was done on pad 15 and 3, whereas the anode was contacted on pad 16 and 2. For cell 2, the cathode was contacted on pad 3 and 7 and the anode on pad 4 and 6 and vice versa for solar cell 3 and 4. First $I-V$ curves for illuminated devices were recorded between −1 and 1 V, and then $I-V$ curves between −2 and 2 V were recorded in the dark.

The conditions of the characterization under simulated sunlight were KHS 575 using a solar simulator from Steuernagel Lichttechnik operating at 1000 W m^{-2}, AM1.5G. The spectrum of the solar simulator was checked using an optical spectrum analyzer made for measuring irradiance, and its intensity was calibrated bolometrically using a precision spectral pyranometer from Eppley Laboratories. During measurements, the incident light intensity was monitored continuously using a CM4 high-temperature pyranometer from Kipp & Zonen.

IPCE measurements were performed using a homemade LED -based illumination system with 18 different wavelengths in the 400−1000 nm range.

UV−vis absorption spectra of the solar cells were recorded in a reflection geometry employing an Avantes CCD UV−vis spectrometer (range 150 to 1100 nm), a Halogen/Deuterium light source (AVA-AVALIGHT-DH) and a seven-furcated (AVA-FCR-7UV200) fiber optics reflection probe with an adjustable collimating lens.

These measurements were performed in an automated setup handling up to 12 substrates at a time, and hence 44 solar cells on 11 substrates were recorded in a single run employing a freshly evaporated Al mirror as reference. Contrary to the automated procedure used in ref 21. the reflection probe used here is within 1−2 cm of the substrate, which renders geometrical corrections less critical. The absorption measurement probed a circular spot with a diameter of ~3 mm and all solar cells were probed at exactly the same position.

RESULTS AND DISCUSSION

General Trends in Photovoltaic Key Values. Figures 1A−3A show scatter plots of J_{sc}, V_{oc}, and FF versus the power conversion efficiency (η) as measured for PT:PCBM and PT:bis-PCBM solar cells in batches PT[1−4]. In Figures 1B−3B, the corresponding results are shown for P3MHOCT:PCBM and P3MHOCT:bis-PCBM solar cells in batches P3MHOCT[1−4]. All data points relating to PT and P3MHOCT are shown with circles in Figure 1−3. Filled symbols designate PCBM and empty symbols bis-PCBM. The batch numbering is indicated by different colors, i.e., black, red, green, and gray designate batches 1−4, respectively.

For reference, the same type of data is shown in Figures 1−3 for the P3HT:PCBM and P3HT:bis-PCBM solar cells made in batches P3HT[1−4]. This data is shown with stars (filled for PCBM and empty for bis-PCBM) and the same color coding as used for PT and P3MHOCT. Note that the same P3HT data are shown in both A and B figures. The corresponding average values, standard deviations and extreme values of η, J_{sc}, V_{oc}, and FF are compiled in Tables 1 and 2.

From Figure 1, it is seen that P3MHOCT solar cells generally give larger J_{sc} than the corresponding PT solar cells and that this is generally also reflected in η. Comparing with the P3HT reference solar cells on average half the value of J_{sc} can be achieved with P3MHOCT as generally also reflected by the efficiencies.

In terms of V_{oc}, from Figure 2 and Table , the performance of P3MHOCT:PCBM cells appears comparable to that of PT:PCBM cells. With bis-PCBM however, on average V_{oc} is ~100 mV larger for PT than for P3MHOCT cells. Despite the considerable spread in V_{oc} it is noteworthy that several PT:bis-PCBM solar cells (from different batches) have a V_{oc} approaching 1 V, which is unprecedented considering that their efficiency is in the range of 0.6%. In other studies

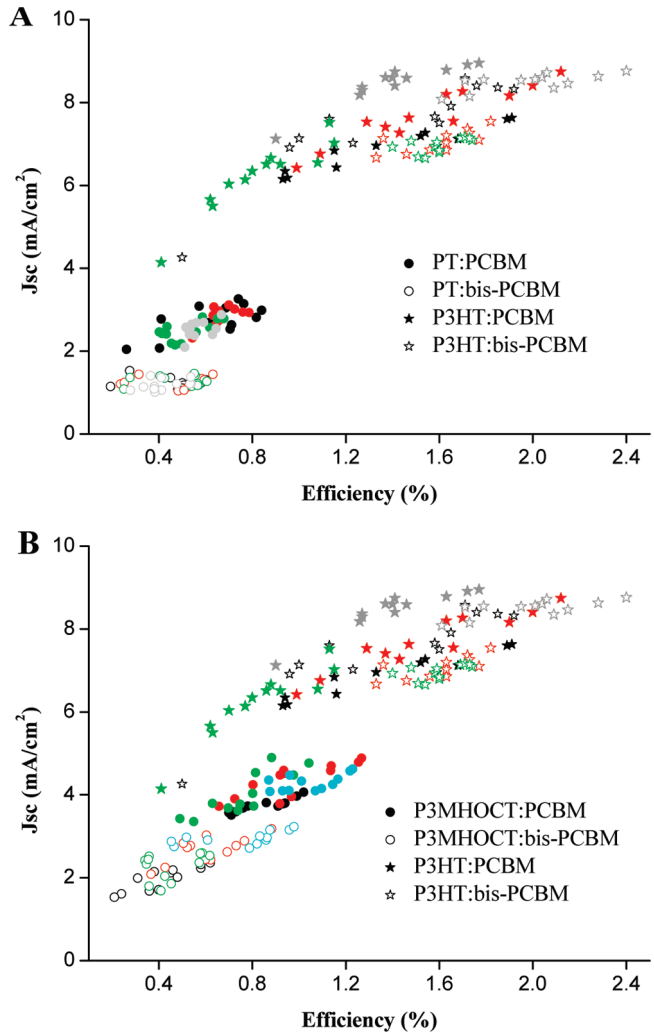

FIGURE 1. Short circuit current density (J_{sc}) as a function of the power conversion efficiency (η) for different production batches 1 to 4 of (A) PT:PCBM and PT:bis-PCBM and (B) P3MHOCT:PCBM and P3MHOCT:bis-PCBM solar cells. Batch numbers are shown with different colors. Results obtained with PCBM are shown with filled symbols, whereas results obtained for bis-PCBM are shown with open symbols. The corresponding results obtained for P3HT:PCBM and P3HT:bis-PCBM (same color coding) solar cells are shown for reference.

where a V_{oc} approaching 1 V was observed, the corresponding efficiency is much lower (22). Compared to P3HT, both PT and P3MHOCT solar cells on average yield higher V_{oc} for both PCBM and bis-PCBM.

In terms of the FF, on average PT:bis-PCBM cells perform much better than the P3MHOCT:bis-PCBM solar cells, as seen from Figure 3 and Table 2. For PT:PCBM and P3MHOCT:PCBM however, on average both the V_{oc} and FF are comparable. On average, the FF for all solar cells employing PCBM are in the same range as seen from Table 1. However, for solar cells employing bis-PCBM, on average PT cells give higher FF than for P3HT cells, which again give higher FF than observed for P3MHOCT cells.

Overall, the P3MHOCT solar cells have higher efficiencies than the PT cells, the performance difference being most outspoken for PCBM, and entirely due to higher J_{sc} values for the P3MHOCT solar cells. In terms of efficiency, both PT and P3MHOCT are inferior compared to P3HT. This is

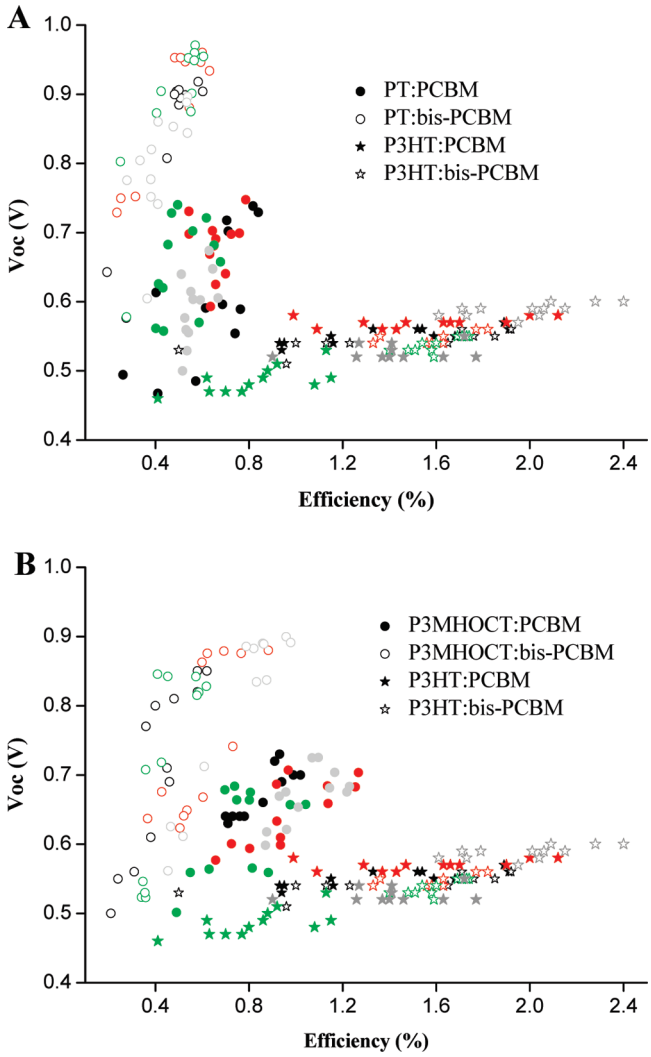

FIGURE 2. Open circuit voltage (V_{oc}) as a function of the power conversion efficiency (η) for different production batches 1 to 4 of (A) PT:PCBM and PT:bis-PCBM and (B) P3MHOCT:PCBM and P3MHOCT:bis-PCBM solar cells. Batch numbers are shown with different colors. Results obtained with PCBM are shown with filled symbols, whereas results obtained for bis-PCBM are shown with open symbols. The corresponding results obtained for P3HT:PCBM and P3HT:bis-PCBM (same color coding) solar cells are shown for reference.

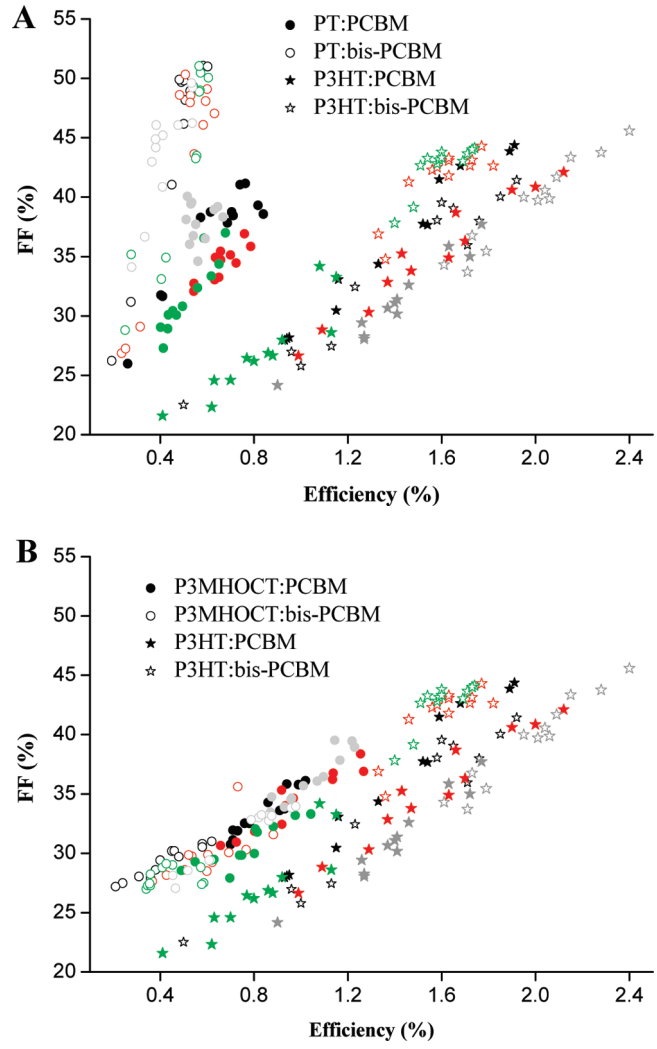

FIGURE 3. Fill factor (FF) as a function of the power conversion efficiency (η) for different production batches 1 to 4 of: (A) PT:PCBM and PT:bis-PCBM and (B) P3MHOCT:PCBM and P3MHOCT:bis-PCBM solar cells. Batch numbers are shown with different colors. Results obtained with PCBM are shown with filled symbols whereas results obtained for bis-PCBM are shown with open symbols. The corresponding results obtained for P3HT:PCBM and P3HT:bis-PCBM (same color coding) solar cells are shown for reference.

mainly due to the significantly larger photo currents of the P3HT solar cells as clearly seen from Figure 1.

When comparing the performance of PCBM and bis-PCBM solar cells, from Figures 1— and Tables 1 and 2, it is found that PCBM is the better choice of acceptor material for PT and P3MHOCT, mainly by virtue of higher J_{sc} values. Even the higher V_{oc} obtained for PT:bis-PCBM cannot compensate the decrease in J_{sc} when replacing bis-PCBM with PCBM. Conversely, for P3HT solar cells bis-PCBM is the better choice of acceptor material due to increased J_{sc} and FF, as seen from Table 1 and 2.

The best material combination in this study is P3MHOCT:PCBM with a peak and average efficiency of 1.3 and 0.9%, respectively. However, this is still clearly below the efficiencies obtained for the reference P3HT solar cells, which for PCBM yields peak and average efficiencies of 2.12 and 1.29% and for bis-PCBM yield 2.40 and 1.65%, respectively. In terms of V_{oc} 1 V has been approached by a peak value of 0.97 V as measured for some PT:bis-PCBM solar cells.

The scatter plot data representation in Figure 1—3 reveals how η correlates with J_{sc}, V_{oc}, and FF. In general terms Figure 3 shows that for all solar cells there is a linear correlation between η and FF. From Figure 2 the picture for V_{oc} seems less clear for PT and P3MHOCT solar cells whereas for P3HT cells there is a clear linear correlation between V_{oc} and η. Figure 1 shows clear correlations between η and J_{sc} for both P3MHOCT and P3HT solar cells.

These correlations indicate which photovoltaic parameters influence the device efficiency by virtue of variations in the processing parameters which are beyond our control. For example, Figure 1B shows that the fluctuation in some experimental condition may influence J_{sc} in the P3MHOCT:bis-PCBM case, such that if J_{sc} is large for a given solar cell then also η becomes large. Conversely, from Figure 1A is seen that in case of PT:bis-PCBM the J_{sc} is virtually un-

Table 1. Average, Standard Deviation, and Maximum and Minimum Key PV Values As Obtained for PT, P3MHOCT, and P3HT Solar Cells Employing PCBM as the Acceptor Material

	η (%)			V_{oc} (V)			J_{sc} (mA/cm^2)			FF (%)		
	PT	P3MHOCT	P3HT	PT	P3MHOCT	P3HT	PT	P3MHOCT	P3HT	PT	P3MHOCT	P3HT
avg	0.59	0.90	1.29	0.63	0.65	0.53	2.65	4.09	7.31	35.22	33.64	32.22
std	0.12	0.19	0.40	0.08	0.05	0.04	0.31	0.42	1.07	3.75	2.9	5.94
max	0.84	1.27	2.12	0.75	0.73	0.58	3.26	4.90	8.95	41.16	39.53	44.38
min	0.26	0.49	0.41	0.47	0.50	0.46	2.04	3.36	4.14	25.98	27.90	21.57

Table 2. Average, Standard Deviation, Maximum and Minimum Key PV Values As Obtained for PT, P3MHOCT, and P3HT Solar Cells Employing bis-PCBM as the Acceptor Material

	η (%)			V_{oc} (V)			J_{sc} (mA/cm^2)			FF (%)		
	PT	P3MHOCT	P3HT	PT	P3MHOCT	P3HT	PT	P3MHOCT	P3HT	PT	P3MHOCT	P3HT
avg	0.46	0.56	1.65	0.86	0.74	0.55	1.23	2.47	7.50	43.61	29.71	39.40
std	0.12	0.20	0.33	0.11	0.13	0.02	0.13	0.46	0.85	7.57	2.18	5.27
max	0.63	0.98	2.40	0.97	0.90	0.60	1.53	3.23	8.76	51.07	35.61	45.57
min	0.19	0.21	0.50	0.58	0.50	0.51	1.01	1.53	4.26	26.22	26.98	22.49

changed under these same process conditions and corresponding unintended parameter variations. In the latter case the spread in η comes about mainly through a correlation between η and FF as seen in Figure 3A.

Performance of the Best Solar Cells. Figure 4 shows the $I-V$ curves for the best performing solar cells under illumination for each material combination employed. To a large extent, these $I-V$ curves are representative of the well-performing solar cells in all the production batches and Figure 4 is therefore used for a general discussion.

Figure 4 underscores two trends seen for PT and P3MHOCT in Figures 1−3; first, that on substituting PCBM with bis-PCBM, V_{oc} increases but with a significant sacrifice in J_{sc} (about a factor of 2), and second, that cleaving P3MHOCT to PT also reduces J_{sc} (again by a factor two). A lowering in J_{sc} could arise from decreased driving force for the initial charge separation, increased bulk-recombination (decreased mobilities and/or unfavorable morphology), decreased light harvesting in the photoactive layer, or the introduction of an electrical barrier. The fact that the $I-V$ curves in Figure 4 display nearly the same slope under reverse bias may point to that bulk-recombination alone is not responsible for the lowing of J_{sc} on replacing PCBM with bis-PCBM and on cleaving P3MHOCT to PT. Admittedly, the solar cells should be characterized under much larger reverse bias conditions for this statement to be firm. We refrained from this, however, because we observed bubble formation in the films when going to −2 V under illumination.

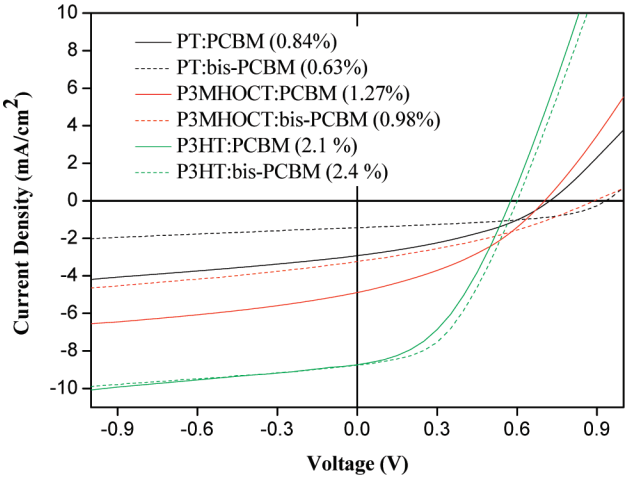

FIGURE 4. $I-V$ curves for the best solar cells obtained for PT and P3MHOCT under illumination. For reference is shown the corresponding curves obtained for P3HT.

The introduction of an electrical barrier on cleaving P3MHOCT to PT or by replacing PCBM with bis-PCBM can also be ruled out because inflection points were never observed in the $I-V$ curves (12, 23–25). In fact, when going from P3MHOCT:PCBM to PT:PCBM and from PT:PCBM to PT:bis-PCBM, the FF increases. Hence, the reduced J_{sc} must come about either by diminished light harvesting or decreased driving force for initial charge separation.

Substituting PCBM with bis-PCBM for the P3HT reference solar cells only leads to a small increase in V_{oc} and FF, and hardly any change in J_{sc}. The $I-V$ curves for the P3HT solar cells can be taken as a measure of what happens when shifting the acceptor LUMO energy (ε_a^L) up by ∼ 0.1 eV (PCBM → bis-PCBM) while keeping the driving force for initial charge separation constant. That is to say, the energy difference between the donor and acceptor LUMO ($\varepsilon_d^L - \varepsilon_a^L$) is such (∼ 0.7 eV or more) that changing ε_a^L by 0.1 eV will not affect the overall driving force for charge separation in the P3HT case. Therefore, J_{sc} is unchanged as seen from Figure 4, but a small increase in V_{oc} and FF results. From Tables 1 and 2, we confirm that this is also in line with the average performance numbers. Note that this is in contradiction with the original paper introducing P3HT:bis-PCBM solar cells, where a ∼0.2 V increase in V_{oc} was ascribed to the substitution of PCBM with bis-PCBM (18). For P3MHOCT and PT, an increase in V_{oc} in the range of 0.2 V can also be observed as seen from Figure 4. From the average numbers in Table 1 and 2, the increase in V_{oc} amounts to ∼0.1 and ∼0.2 V for P3MHOCT and PT, respectively. In the latter case, an increase of 0.2 V cannot simply be rationalized in terms of HOMO LUMO energies, and a more complex mechanism must be at work.

Going from P3HT over P3MHOCT to PT, the optical band gap is largely unchanged as confirmed in Figure S1 of the

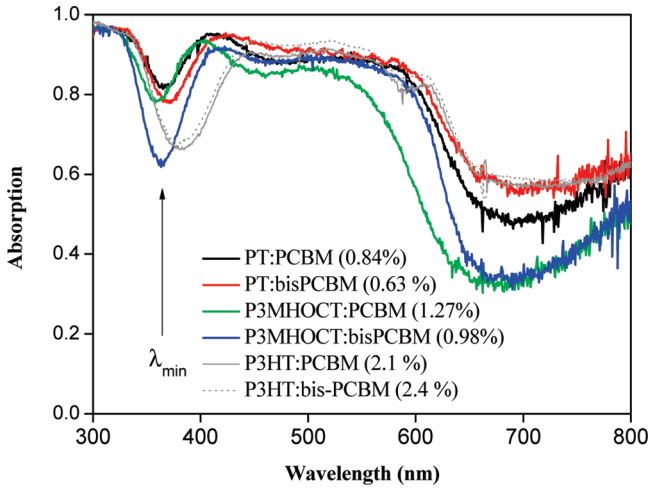

FIGURE 5. UV−vis absorption spectra recorded for the best performing PT and P3MHOCT solar cells. The approximate position of λ_{min} is indicated by an arrow. The corresponding results are shown for the best performing P3HT solar cells.

Supporting Information, whereas the donor HOMO level (ε_d^H) is shifted substantially downward, at least in the case of P3MHOCT (26). From preliminary CV experiments on identically prepared films of P3HT:PCBM, P3MHOCT:PCBM, and PT:PCBM (see Figure S2 in the Supporting Information), an ~600 meV shift of the first oxidation potential is observed on going from P3HT to P3MHOCT. The corresponding decrease in $\varepsilon_d^L-\varepsilon_a^L$ for P3MHOCT:PCBM compared to P3HT:PCBM therefore implies a decrease in J_{sc} in the former case. Because for P3MHOCT:PCBM ε_d^L and ε_a^L are quite close in energy, J_{sc} becomes susceptible to even small changes in ε_a^L as, for example, induced by substituting PCBM by bis-PCBM. This might explain why J_{sc} is abruptly halved on replacing PCBM with bis-PCBM in case of P3MHOCT, but not in the case of P3HT. For PT the CV results (see Figure S2 in the Supporting Information) are less conclusive and thus we can not rationalize the decrease in J_{sc} on going from P3MHOCT to PT based on the HOMO LUMO energies. Experimentally, however, this decrease could be ascribed to the thermal treatment leading to PT. Indeed we made the general observation that prolonged heating during the cleaving step only leads to a lowering of the efficiency for the PT solar cells, and consequently this step was kept as short as possible. In practice, this amounts to a few seconds, and within this time we cannot trace any sign of decomposition of either PEDOT:PSS or the PCBM/bis-PCBM as inquired by UV−vis spectroscopy, AFM, thermogravimetric analysis, and differential scanning calorimetry (see Figures S3−S6 in the Supporting Information). However, from AFM measurements performed on P3MHOCT:PCBM films before and after thermal cleaving (see Figure S7 in the Supporting Information), it is seen that both the interface roughness and domain size changes. To assess if this morphology change gives rise to changes in charge carrier mobilities, we attempted to derive hole mobilities from FET devices prepared from P3MHOCT and PT. However, because of pronounced contact resistances, these preliminary results were not conclusive.

In Figure 5, the UV−vis absorption spectra as measured for the best performing solar cells are shown. Again, these may be taken as representatives for the remaining set of solar cells in the respective production batches. Note that these spectra are recorded for the entire solar cell in reflection geometry and thus are very sensitive films imperfections and opaqueness. The absorption spectra cannot be used to assess the light harvesting potential (in terms of an upper limit to the photo current) of the photoactive layer itself. Nonetheless, by comparisons of the spectra in Figure 5, it may still be loosely argued that the differences in J_{sc} (Table 1 and 2) seen for different material combinations, most likely is not of an optical origin as the spectra appear rather similar. This is seen on comparing the absorption spectra for the PT:bis-PCBM and P3HT:bis-PCBM solar cells. Apart from the 300−400 nm range, these spectra are nearly identical and yet, on average, J_{sc} is six times larger in the P3HT case. Also, the fact that the spectrum for P3MHOCT:PCBM in Figure 5 cuts off at shorter wavelengths than for the remaining three material combinations, contradicts that P3MHOCT:PCBM solar cells display the largest values of J_{sc} among the P3MHOCT and PT solar cells.

The absorption spectra in Figure 5 do not reflect the trends seen for the Incident Photo to Current Conversion Efficiency (IPCE) as measured for the different material combinations (see Figure S8 in the Supporting Information). This again supports the assumption that it is not the light-harvesting properties of the materials per se that give rise to reduced J_{sc} on replacing PCBM with bis-PCBM or when cleaving P3MHOCT to PT.

An important characteristic is the minimum between 300 and 400 nm, the position of which is indicated in Figure 5 and designated as λ_{min}. As previously shown for P3HT:PCBM solar cells, a linear correlation between the thickness of the photoactive layer and the position of a certain distinct minimum in the UV−vis absorption spectrum of the entire solar cell can be established (21). Because the first absorption minimum in Figure 5 is very sensitive to changes in the photoactive layer thickness, it is possible to correlate thickness and λ_{min} in a similar fashion as done in ref 21.

Hence in Figure 6, the average position of λ_{min} versus the average thickness of the photoactive layer is shown for solar cells in the four extra batches where the spin-coating speed was varied (a batch each for PT:PCBM, PT:bis-PCBM, P3MHOCT:PCBM, and P3MHOCT:bis-PCBM). Clearly, four linear correlations between λ_{min} and the thickness of the photoactive layer have been obtained, and the parameters corresponding to the best linear fit of the data are shown in Figure 6.

Spread of the Photovoltaic Data. Figures 1−3 reveal a notable spread in the measured $I-V$ data. In terms of η, the standard deviation obtained for P3MHOCT cells is almost twice the standard deviation calculated for PT cells. This is due to a larger spread in J_{sc} for P3MHOCT than for PT cells. However, for the P3HT solar cells, the spread in η is larger than for both PT and P3MHOCT by virtue of a substantial spread in J_{sc} and/or FF.

Figure 2 shows a substantial spread in V_{oc} for the PT and P3MHOCT solar cells compared to the P3HT reference solar

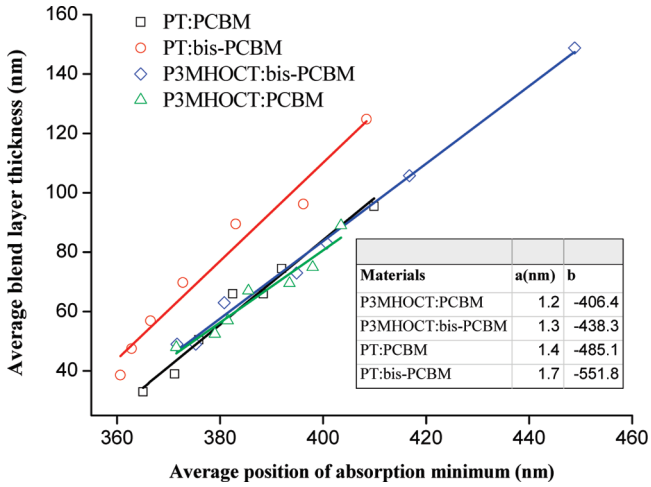

FIGURE 6. Average blend layer thickness as measured by AFM as a function of the average position of λ_{min} for PT and P3MHOCT solar cells. Also shown are the best linear fit of the data for the four types of solar cells described the relation $d = a + b\lambda_{min}$. The values of a and b as obtained for the different material combinations are shown in the inset table.

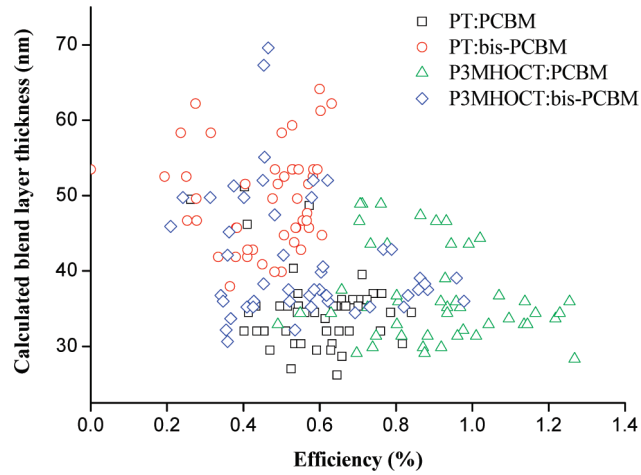

FIGURE 7. Thickness of the active layer for all PT:PCBM, PT:bis-PCBM, P3MHOCT:PCBM, and P3MHOCT:bis-PCBM solar cells as a function of their efficiency. The thickness is derived from λ_{min} as obtained from the UV−vis absorption spectrum of each cell.

cells which display a quite small spread in V_{oc}. Most notably is the large spread for the PT:bis-PCBM and P3MHOCT:bis-PCBM solar cells as also confirmed by Tables 1 and 2. From Figure 3 and Tables 1 and 2, a comparable spread in FF is seen for PT:PCBM and P3MHOCT solar cells. The PT:bis-PCBM solar cells display the largest spread in FF, even larger than that of the P3HT solar cells. It should be noted that the relatively low values obtained for FF in this study generally can be ascribed to the substrate layout which was designed mainly with reproducibility in mind. Improved FF values can be achieved by employing smaller active areas and/or Au busses on the substrate prior to processing. However, we have refrained from this to avoid areas on the substrate with wetting properties different from ITO, as this may affect the film uniformity.

It is noteworthy that the PT:bis-PCBM solar cells with an average efficiency of 0.46% display the smallest spread in J_{sc} but the largest spread in FF as seen from Table 2. Among all solar cells, the PT cells also display the smallest spread in efficiency. Considering their manufacturing process, a priori a larger spread in η could have been expected because PT cells are subject to a thermal cleaving step, inherently difficult to perform in a strictly reproducible way. However, the opposite trend is observed, and in fact η is less reproducible for the P3MHOCT, and in particular P3HT solar cells.

From the scatter plots in Figure 1−3 clustering of data points belonging to the same production (i.e., data points of same color) batch is not observed. Thus, whatever influential production parameters are causing spread in the $I-V$ data, the fluctuations in these parameters occur also while processing substrates belonging to the same evaporation batch. Hence, the batchwise spread is not due to variations in the Al deposition conditions.

The spread in the $I-V$ data may also be considered at the substrate level, i.e., the variability of the $I-V$ data for solar cells on the same substrate. In principle, the four solar cells on a substrate are subject to exactly the same process conditions, and by virtue of the substrate design all four solar cells also experience identical electrical surroundings. The substratewise spread can therefore only be ascribed to nonuniformity of the different thin-film layers and/or intrinsic morphology/interface nonuniformities. The substratewise (or residual) spread can be assessed by carefully inspecting the scatter plots in Figures 1−3, where it is seen that the 12 symbols of a given color only occasionally appear in groups of four.

To assess if the spread in the $I-V$ data in Figures 1−3 (including the residual spread) is linked to variations of the photoactive layer thickness, this thickness was calculated for all solar cells based on their absorption spectra. This was done using λ_{min} and the linear relations given in the inset in Figure 6 for PT and P3MHOCT. Knowing the thickness of the photoactive layer of each solar cell, the IV data may then be investigated for correlations with respect to the thickness. Hence, in Figure 7, a scatter plot of the calculated thickness versus efficiency is shown for all the PT and P3HMOCT solar cells. No correlation between η and the layer thickness of the photoactive layer is seen for any of the material combinations investigated. Similar scatter plots of the photoactive layer thickness versus J_{sc}, V_{oc}, and FF (not shown) were scrutinized and no correlations found either. Also for the reference P3HT solar cells where the spread is quite substantial, no correlation between η and blend layer thickness was found (see Figure S9 in the Supporting Information). To this end, it should be emphasized that a significant effort was made to ensure that for all material combinations uniform films could be accomplished repeatedly. In fact, the particular choice of P3HT blend formulation and spin-coating conditions was made in order to obtain as uniform films as possible and not in order to optimize device efficiency. Therefore, chlorobenzene was used for the processing of the P3HT solar cells and not o-dichlorobenzene, because in the latter case highly uniform films could not be accomplished.

The solar cells have very uniform films and to a large extent the measured absorption spectrum (always probed at the same location but for a limited area of the solar cell)

can be taken as representative of the whole cell. Hence, the spread in the IV data for solar cells produced under seemingly identical conditions is neither of optical origin nor coupled to variations in the blend layer thickness.

In terms of the substrate-wise spread in the IV data, the only remaining possible causes of it can be variations of the local film morphology and/or interfaces properties, both of which only impact the electrical properties of the solar cells. The fact that the solar cells of this study feature an active area ~38 times larger than that used in ref (19) (ten P3HT:PCBM solar cells 5.3 mm^2 each on a substrate) apparently does not decrease the spread in the IV data by virtue of averaging local variations out. Also, the fact that we use an ITO pattern on the substrate that allows for an uninterrupted blend flow while spin coating, contrary to the structured ITO used in ref (19), seems not to diminish the spread in the IV data. Hence, the active area and ITO patterning are not decisive in terms of the spread in the IV data as sometimes speculated.

Film Morphology. To further pursue the question of why solar cells from the same process batch, or even from the same substrate, can display so different solar cell performance, we conducted several AFM measurements for P3MHOCT and PT solar cells with good and poor efficiencies from the same batch. Figure S10 shows an example of such AFM measurements for P3MHOCT:PCBM and PT:PCBM solar cells, from which it is clear that no significant roughness or morphology features characterize good or poor device performance. We should stress that such measurements by nature are not representative since only a restricted region on a limited number of devices are probed in practice, and because the region probed lies between the solar cells (inside the ITO area) where no Al contact has been deposited.

CONCLUSION

By a comparative study of solar cells employing the thermo-cleavable polymer P3MHOCT and its cleaved end product PT it was shown that V_{oc} can increase significantly when substituting PCBM with bis-PCBM. In the case of PT:bis-PCBM, V_{oc} approaching 1 V was obtained for several solar cells which is unprecedented considering their efficiencies being in the 0.6% range. However, this substitution of acceptor material involves a sacrifice in J_{sc} which amounts to a factor two, and overall the optimal material combination remains P3MHOCT:PCBM with a peak efficiency of 1.3%. Based on the IV data for cells under illumination, the photovoltaic behavior of solar cells with the different material combinations to some extent could be rationalized in terms of simple considerations of HOMO and LUMO energy levels. However, the rather large increase in V_{oc} for PT and P3MHOCT upon substituting PCBM with bis-PCBM, and as *not* seen for the corresponding P3HT solar cells, can not be rationalized in such simple terms. Despite the effort and special measures taken in terms of substrate design, characterization and process standardization, a significant scatter in the photovoltaic key parameters was generally observed. The smallest spread in the photovoltaic efficiency was observed for PT solar cells which however also featured the lowest efficiencies. The largest spread was clearly seen for the P3HT reference solar cells which however gave rise to highest photovoltaic efficiencies.

Generally, a residual spread in the IV data for solar cells on the same substrate was observed. Combined with the absence of correlations between the photovoltaic parameters and the thickness of the photoactive layer indicates that at least one possible cause of the variability for the IV data should not be ascribed to the unintended variation of the processing parameters as the inevitabe part of the manual making (lab scale) of polymer solar cells.

Acknowledgment. This work was supported by the Danish Strategic Research Council (DSF 2104-05-0052 and 2104-07-0022). We would like to thank Torben Kjær and Jan Asltrup for technical assistance, Noemi Rozlosnik for assisting with the AFM measurements and Ole Hammerich for assisting with the CV measurements.

Supporting Information Available: Transmission spectra of the blend materials subject to different process conditions, Cyclic voltammogram for P3HT:PCBM, P3MHOCT:PCBM and PT:PCBM as measured on ITO glass, Transmission spectra for PEDOT:PSS on ITO glass subject to different process conditions, AFM images of PEDOT:PSS before and after annealing at 310 °C, Transmission spectra for PCBM and bis-PCBM on float glass before and after an annealing at 310 °C, TGA and DSC for PCBM and bis-PCBM, AFM images of P3MHOCT:PCBM and PT:PCBM on float glass, IPCE measurements for all the material combinations investigated and scatter plot of the thickness of the active layer for all P3HT based solar cells versus their efficiency (PDF). This material is available free of charge via the Internet at http://pubs.acs.org.

REFERENCES AND NOTES

(1) Hoppe, H.; Sariciftci, N. S. *J. Mater. Chem.* **2006**, *16*, 45–61.
(2) Günes, S.; Neugebauer, H.; Sariciftci, N. S. *Chem. Rev.* **2007**, *107*, 1324–1338.
(3) Bundgaard, E.; Krebs, F. C. *Sol. Energy Mater. Sol. Cells* **2007**, *91*, 954–985.
(4) Jørgensen, M.; Norrman, K.; Krebs, F. C. *Sol. Energy Mater. Sol. Cells* **2008**, *92*, 686–714.
(5) Thompson, B. C.; Fréchet, J. M. J. *Angew. Chem., Int. Ed.* **2008**, *47*, 58–77.
(6) Hadipour, A.; de Boer, B.; Blom, P. W. M. *Adv. Funct. Mater.* **2008**, *18*, 169–181.
(7) Ameri, T.; Dennler, G.; Lungenschmied, C.; Brabec, C. J. *Energ. Environ. Sci.* **2009**, *2*, 347–363.
(8) Hagemann, O.; Bjerring, M.; Nielsen, N. C.; Krebs, F. C. *Sol. Energy Mater. Sol. Cells* **2008**, *92*, 1327–1335.
(9) Han, X.; Chen, X.; Holdcroft, S. *Adv. Mater.* **2007**, *19*, 1697–1702.
(10) Liu, J. S.; Kadnikova, E. N.; Liu, Y. X.; McGehee, M. D.; Fréchet, J. M. J. *J. Am. Chem. Soc.* **2004**, *126*, 9486–9487.
(11) Krebs, F. C.; Spanggaard, H. *Chem. Mater.* **2005**, *17*, 5235–5237.
(12) Krebs, F. C.; Norrman, K. *Prog. Photovoltaics: Res. Appl.* **2007**, *15*, 697–712.
(13) Krebs, F. C. *Sol. Energy Mater. Sol. Cells* **2008**, *92*, 715–726.
(14) Bjerring, M.; Nielsen, J. S.; Siu, A.; Nielsen, N. C.; Krebs, F. C. *Sol. Energy Mater. Sol. Cells* **2008**, *92*, 772–784.
(15) Krebs, F. C.; Thomann, Y.; Thomann, R.; Andreasen, J. W. *Nanotechnology* **2008**, *19*, 424013.
(16) Bjerring, M.; Nielsen, J. S.; Nielsen, N. C.; Krebs, F. C. *Macromolecules* **2007**, *40*, 6012–6013.
(17) Gevorgyan, S. A.; Krebs, F. C. *Chem. Mater.* **2008**, *20*, 4386–4390.
(18) Lenes, M.; Wetzelaer, G.-J. A. H.; Kooistra, F. B.; Veenstra, S. C.; Hummelen, J. C.; Blom, P. W. M. *Adv. Mater.* **2008**, *20*, 2116–2119.

(19) Riede, M. K.; Sylvester-Hvid, K. O.; Glatthaar, M.; Keegan, N.; Ziegler, T.; Zimmermann, B.; Niggemann, M.; Liehr, A. W.; Willeke, G.; Gombert, A. *Prog. Photovoltaics: Res. Appl.* **2008**, *16*, 561–576.
(20) Krebs, F. C.; Jørgensen, M.; Norrman, K.; Hagemann, O.; Alstrup, J.; Nielsen, T.; Fyenbo, J.; Larsen, K.; Kristensen, J. *Sol. Energy Mater. Sol. Cells* **2009**, *93*, 422–441.
(21) Sylvester-Hvid, K. O.; Ziegler, T.; Riede, M. K.; Keegan, N.; Niggemann, M.; Gombert, A. *J. Appl. Phys.* **2007**, *102*, 054502.
(22) Peng, Q.; Park, K.; Lin, T.; Durstock, M.; Dai, L. *J. Phys. Chem. B* **2008**, *112*, 2801–2808.
(23) Glatthaar, M.; Riede, M.; Keegan, N.; Sylvester-Hvid, K. O.; Zimmermann, B.; Niggemann, M.; Hinsch, A.; Gombert, A. *Sol. Energy Mater. Sol. Cells* **2008**, *91*, 390–393.
(24) Vogel, M.; Doka, S.; Breyer, M.; Lux-Steiner, C.; Fostiropoulos, K. *Appl. Phys. Lett.* **2006**, *89*, 163501.
(25) Zhang, S. T.; Zhou, Y. C.; Zhao, J. M.; Zhan, Y. Q.; Wang, Z. J.; Wu, Y.; Ding, X. M.; Hou, X. Y. *Appl. Phys. Lett.* **2006**, *89*, 043502.
(26) Murphy, A. R.; Liu, J.; Luscombe, C.; Kavulak, D.; Frechet, J. M. J.; Kline, R. J.; McGehee, M. *Chem. Mater.* **2005**, *17*, 4892–4899.

AM900518R